

Lectures on Superconducting Quantum Circuits

Notes - v. 1.0

Federica Mantegazzini

fmantegazzini@fbk.eu
f.mantegazzini@unitn.it

University of Trento
24-26 March 2025

Contents

1	Introduction	2
2	Microwave Coplanar Waveguides	3
3	Superconducting Resonators	4
4	Josephson Junctions	7
5	Microwave Tunable Resonators	9
6	Josephson Parametric Amplifiers	12
7	Superconducting Qubits	16

These notes are meant as a summary of the lectures and a helpful tool for the students. They are a living document. Suggestions to improve the content and corrections of typos or possible errors are more than welcome.

1 Introduction

Superconducting circuits have attracted growing interest in the scientific community as a tool to implement quantum optics experiments in the microwave regime as well as a platform for quantum technologies.

Examples of applications of superconducting circuits include:

- *Quantum optics and circuit QED (cQED) experiments*, exploring the fundamental interactions between microwave light and matter;
- *High-resolution cryogenic detectors*, widely used for particle physics experiments (e.g. dark matter and neutrino physics) and astroparticle physics applications (e.g. for telescopes).
- *Quantum sensing*, exploiting the quantum nature of superconductivity to build sensors based on quantum tunnelling, superposition and entanglement phenomena.
- *Quantum computing*, realising superconducting artificial atoms that work as qubits, where the first two energy levels $|0\rangle$ and $|1\rangle$ are used as computational basis.

The key advantage of superconducting circuits as experimental platform for quantum applications is the fact that superconductivity is a *macroscopic quantum phenomenon*. This implies that relatively large, i.e. "macroscopic" superconducting structures, with sizes in the order of tens or hundreds of micrometers, preserve their quantum nature. This feature allows to design and produce circuits, with incredibly high flexibility, to control and exploits quantum phenomena. One example is the transmon qubit, a superconducting circuit widely used as basic building block for superconducting quantum processors, which we will discuss in section 7.

Quantum states are typically very fragile and the environmental disturbances, such as thermal noise, can be detrimental, easily destroying quantum coherence. Superconducting devices are operated at very low temperatures, typically in the order of millikelvin, and in the microwave regime, at frequencies of few GHz. Therefore, it results that the thermal noise $k_B T$ is much lower than the energy scale $\hbar\omega$, with $\omega = 2\pi f$ and $f \approx 5GHz$. This condition:

$$k_B T \ll \hbar\omega \tag{1}$$

is in fact crucial to allow the exploitation of quantum circuits to build qubits and other quantum devices.

Other advantages of the superconducting platform include:

- **Strong light-matter coupling:** In cQED, the interaction between photons and atoms is given by the ratio between the coupling strength and the bare energy of the excitations; with superconducting circuits, very high level of interactions can be achieved, enabling experiments in the strong and ultra-strong regimes;
- **The (quasi) absence of dissipation in superconducting circuits:** Superconductivity allows zero-resistance current flow in the circuit, which brings the dissipation close to zero;
- **Scalability:** Superconducting circuits are typically microfabricated on silicon chips, exploiting cleanroom techniques readily developed by the semiconductor industry, allowing for high control and high scalability.

In these lectures, we will start from the basic components to build a superconducting circuits, namely coplanar waveguides, superconducting resonators and Josephson junctions. By combining this elements in a circuit, a wide range of superconducting quantum devices can be realised. We will discuss two interesting examples of superconducting circuits based on Josephson junctions, namely the Josephson Parametric Amplifier (JPA) and the transmon qubit.

2 Microwave Coplanar Waveguides

In order to build superconducting circuits, we need to be able to transmit microwaves, i.e. electromagnetic waves with frequencies in the order of few GHz, in a controlled way.

In the 3D world, we use coaxial cables to transmit microwaves. A coaxial cable comprises an inner conductor and an outer ground separated by dielectric material, as shown in figure 1.

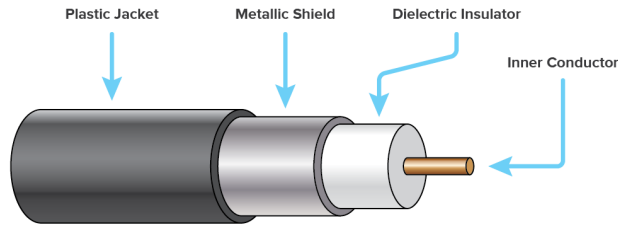


Figure 1: A coaxial cable, comprising the inner conductor, the dielectric insulator, the shield which serves as ground and a plastic jacket which serves as protection.

In a superconducting planar circuit, structures must feature a planar geometry and they are realised exploiting planar microfabrication techniques. Therefore, we need to implement a planar version of a coaxial cable. The simplest planar implementation of a transmission line is the *coplanar waveguide* shown in figure 2. A coplanar waveguide consists of a planar central conductor and a planar ground plane separated from the central conductor by a gap. In a typical superconducting circuit, a superconducting thin film (e.g. an aluminium film with a thickness in the order of 100 nm) is deposited on a silicon substrate and patterned by removing the film from the gap region.

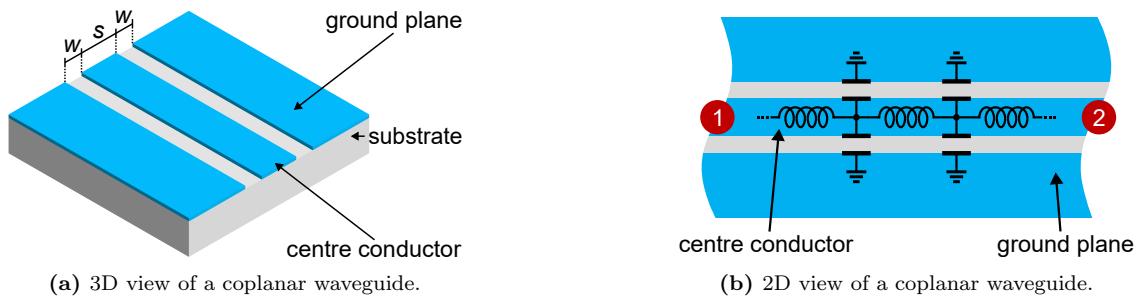


Figure 2: Coplanar waveguide comprising the central conductor and the ground plane.

A coplanar waveguide is characterised by an inductance, given by the geometrical inductance of the central conductor, and by a capacitance, given by the facing metallic planes of the central conductor and the ground.

Therefore, we can define two important parameters of a coplanar waveguide:

- The distributed inductance L' , i.e. the inductance per unit of length;
- The distributed capacitance C' , i.e. the capacitance per unit of length;

To calculate L' and C' , *conformal mapping* techniques are typically exploited. These are algebraic methods which are used to map a complex geometry, such as a coplanar waveguide, to a simpler and known geometry, such as a parallel plate capacitor. In this way it is possible to calculate in a rigorous way L' and C' for a given geometry of a coplanar waveguide. The free parameters for each geometry are the width of the central conductor and the width of the gap between the central conductor and the ground plane.

From the distributed distributed capacitance L' and the capacitance C' , we can calculate the characteristic impedance Z_0 of the waveguide:

$$Z_0 = \sqrt{\frac{L'}{C'}} \quad (2)$$

and the phase velocity v_{ph} of the microwave travelling inside the waveguide:

$$v_{\text{ph}} = \frac{1}{\sqrt{L'C'}} \quad (3)$$

We can visualise the microwave travelling inside the waveguide looking at the electromagnetic field distribution, with the electric component \vec{E} and the magnetic component the electric component \vec{B} , as shown in figure 3.

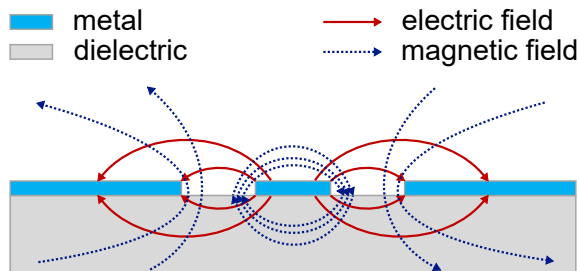


Figure 3: Visualisation of the field distribution of a quasi-TEM mode travelling in a coplanar waveguide.

3 Superconducting Resonators

Starting from coplanar waveguides, we can build planar microwave cavities. To do this, we can exploit interference and superposition effects of microwaves travelling in a waveguide with a certain boundary conditions.

In figure 4, we consider the case of a medium terminated with a closed end, equivalent to a coplanar waveguide terminated to ground. This configuration causes reflection of the electric component of the wave with a phase shift of π . A standing wave in a medium is a resonator: we have built a superconducting microwave resonator.

In the animation¹, we can see how an incoming wave (green) travelling from left to right in a medium is bouncing back when reflected at the end of the medium (right end of the figure). The reflected way (blue) is interfering with the incoming way (green) and the resulting superposition of the two gives a standing wave (red).

Different boundary conditions result in different phase shifts and therefore different standing waves. In particular, we can think to two different configurations, namely the *quarter-wave resonator* and the *half-wave resonator*.

¹<https://upload.wikimedia.org/wikipedia/commons/5/5d/Wavinterference.gif>

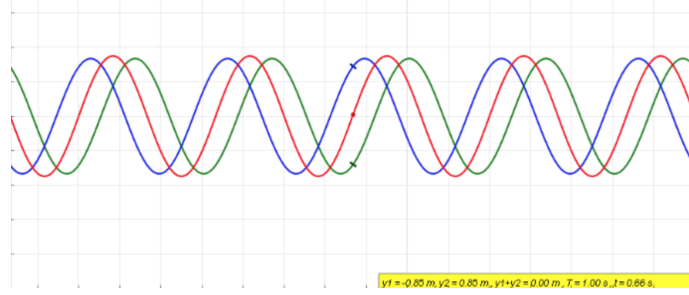


Figure 4: Animation here: <https://upload.wikimedia.org/wikipedia/commons/5/5d/Wavinterference.gif>. The incoming wave (green) is reflected and the back-travelling wave (blue) is interfering resulting in the standing wave (red).

Quarter-wave resonator A coplanar waveguide is interrupted at one end by a capacitor, which prevents current flowing, and is terminated to ground at the other end, allowing maximum current flow, as shown in figure 5a. We therefore have a current node (i.e. zero current, maximum voltage) at one end and a voltage node (i.e. maximum current, zero voltage) at the other end. The electrical components of the microwave is forced to be zero at one end and maximum at the other end. The resulting standing wave is characterised by a wavelength λ which corresponds to four times the length of the resonator l : $\lambda = 4l$. In other words, a quarter of the wave fits in the resonator, hence generating a *quarter-wave* resonator.

Half-wave resonator A coplanar waveguide is interrupted at the two ends by two capacitors, which prevent flowing of current, as shown in figure 5b.. We therefore have two current nodes (i.e. zero current, maximum voltage) at the two ends, forcing the electrical components of the microwave to be zero. The resulting standing wave is characterised by a wavelength λ which corresponds to twice the length of the resonator l : $\lambda = 2l$. In other words, half wave fits in the resonator, hence generating a *half-wave* resonator.

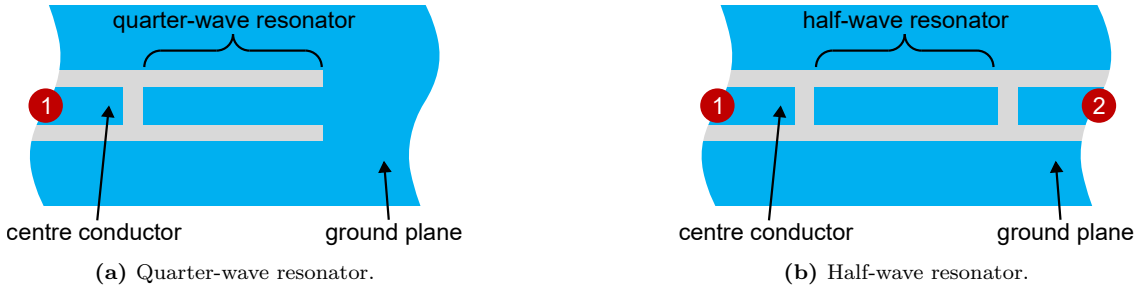


Figure 5: Planar resonators with different boundary conditions. The ports used to probe the resonators with a microwave tone are shown in red.

In figure 6 the quarter-wave (left) half-wave (right) configurations are visualised, including the allowed harmonics. Note that for the quarter-wave resonator only the odd harmonics are allowed by the boundary conditions.

By characterising superconducting resonators with a Vector Network Analyser (VNA), their resonance frequencies can be extracted. A VNA is an RF instrument with two ports, which generates a microwave signal at port i and it compares in terms of amplitude and phase with the signal detected at port j , where $i, j \in \{1, 2\}$. The VNA returns the so called *scatter parameters* S_{ij} . The parameters S_{11} and S_{22} describe the forward and backwards reflections, while S_{21} and S_{12} describe the forward and backwards transmissions (ref Pozar).

Using a VNA, we can probe a **quarter-wave resonator** with a reflection measurement, sending a signal to the port 1 of the device (see figure 5a) and sweeping the frequency of the signal. The

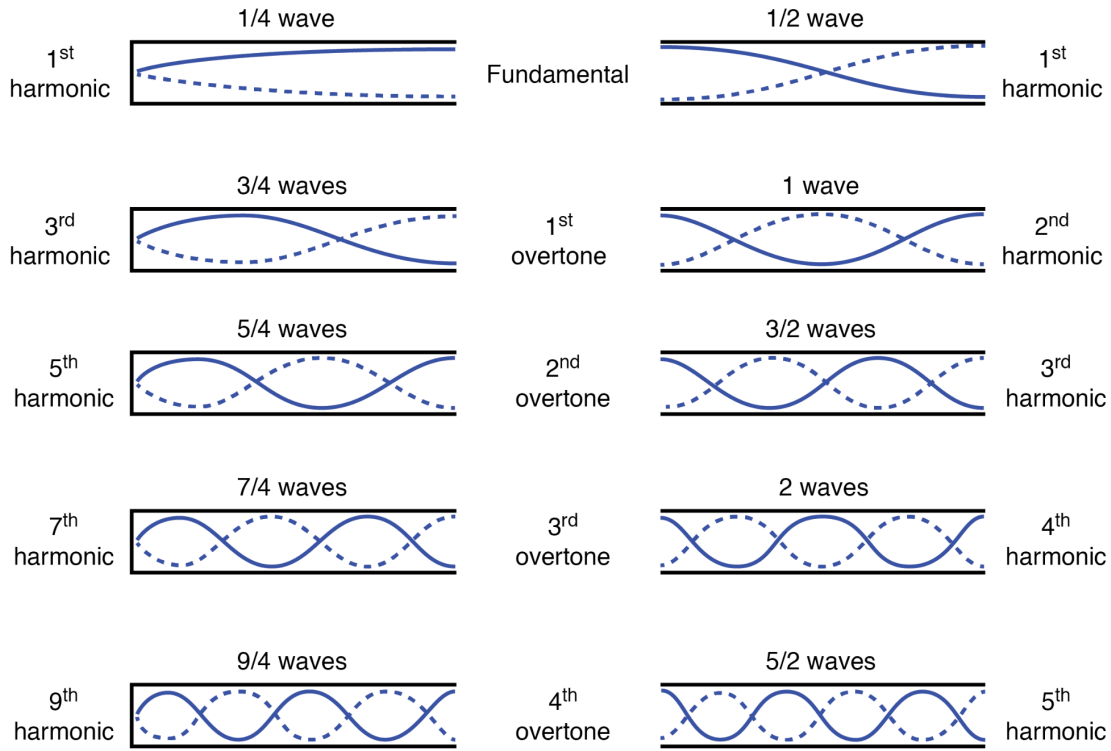


Figure 6: Schematics of the wave fitting in quarter-wave and half-wave resonators and their harmonics.

plot in figure 7a shows the measured reflection as a function of the signal frequency:

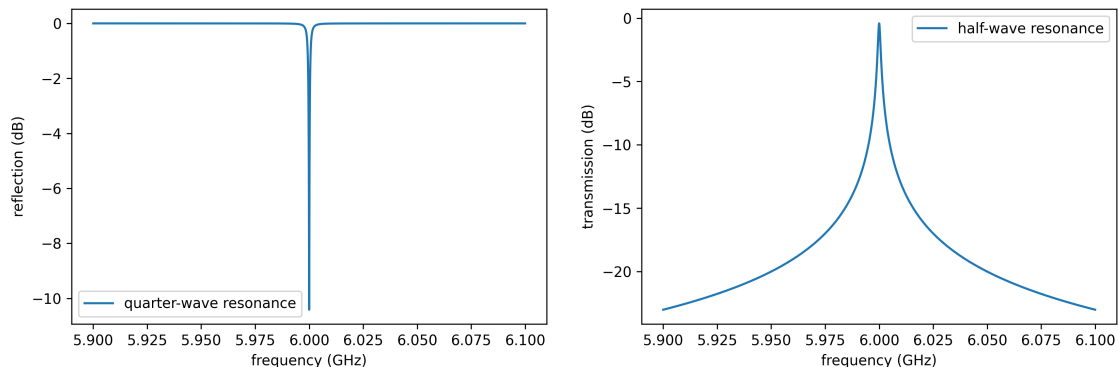
- When the signal frequency does not match the resonance frequency, the reflection is total (i.e. at the maximum of 0 dB = 100% reflection). This happens because the sent microwave cannot fit in the quarter-wave resonator and therefore is entirely reflected back to port 1 of the device.
- When the signal frequency matches the resonance frequency, the reflection is at the minimum, generating a dip in the reflection graph. Under this condition, the microwave can enter the resonator and it is trapped there, so that the reflection is minimal.

Similarly, we can probe a **half-wave resonator** with a transmission measurement, sending a signal to the port 1 of the device and reading the transmission at port 2 of the device (see figure 5b, while sweeping the frequency of the signal. The plot in figure 7b) shows the measured transmission as a function of the signal frequency:

- When the signal frequency does not match the resonance frequency, the transmission is very low (ideally $-\infty$). This happens because the sent microwave cannot fit in the half-wave resonator and therefore is entirely reflected back to port 1 of the device.
- When the signal frequency matches the resonance frequency, the signal can enter the resonator and be transmitted to the other side, generating a peak in the transmission graph. Under this condition, the microwave is trapped inside the resonator and subsequently transmitted both backwards (to port 1 of the device) and forward (to port 2 of the device).

In both cases, reflection and transmission are measured in logarithmic units of dB.

The superconducting resonators that we have reviewed are not tunable and their resonance frequency is fixed by the geometry of the circuit. Moreover, so far the circuit dynamics we have



(a) Response of a quarter-wave resonator.

(b) Response of a half-wave resonator.

Figure 7: Microwave responses of superconducting resonators, showing the resonance frequency.

encountered is fully linear. In order to build interesting circuits for quantum optics and cQED experiments as well as to realise superconducting qubits, we need to introduce tunability and non-linearity in our superconducting circuits. In the superconducting toolbox, we have a special element that behaves as a controllable, dissipationless and tunable non-linear inductance, namely the Josephson junction.

4 Josephson Junctions

The Josephson junction is one of the most important circuit elements in the field of superconducting quantum devices. It consists of a sandwich of two superconducting electrodes separated by a thin insulating barrier which allows coherent tunnelling of Cooper pairs, the charge carriers in a superconductor.

Practically, Josephson junctions are realised overlapping two thin superconducting films, for example ~ 100 nm thick Al films, separated by a ~ 1 nm aluminium oxide barrier. A schematic of a Josephson junction is shown in figure 8.

Josephson equations

To describe the physics of a Josephson junction, we should recall the foundations of the Bardeen – Cooper – Schrieffer (BCS) theory, which describes the phenomenon of superconductivity as the result of the condensation of Cooper pairs. At low temperatures, i.e. when the energy of the system is highly reduced, an attractive potential between electrons is generated which causes binding of electrons into Cooper pairs. Thanks to their bosonic nature, Cooper pairs form a large Bose-Einstein condensate. Under these conditions, the quantum mechanical character of the ground state of the system appears on a macroscopic scale.

As a result, a single wave function $\Psi(x, t)$ can describe a macroscopic number of Cooper pairs that condensate in the same quantum state. We can therefore write a *macroscopic wave function* describing a macroscopic piece of superconductor, such as each superconductor forming a Josephson junction:

$$\Psi(x, t) = \sqrt{\rho} e^{i\phi(x, t)} \quad (4)$$

where ϕ is the common phase and ρ is the density in the macrostate, with $|\Psi|^2 = \rho$.

The time evolution of the macroscopic wave function in stationary conditions follows the Schrödinger equation:

$$i\hbar \frac{\partial \Psi}{\partial t} = H\Psi \quad (5)$$

Bearing this in mind, we can derive the dynamics of a Josephson junction by introducing two macroscopic wave functions Ψ_1 and Ψ_2 for the two superconductors (see figure 8) and using the Schrödinger equation with a coupling term describing the overlap of the wave functions in the barrier. The full derivation is beyond the scope of these lectures and it can be found in Feynman's lecture *The Schrödinger Equation in a Classical Context: A Seminar on Superconductivity* (see the section **Suggested Textbooks and Reviews**).

As a result, the dynamic of a Josephson junction is described by two simple and elegant equations called *Josephson equations*.

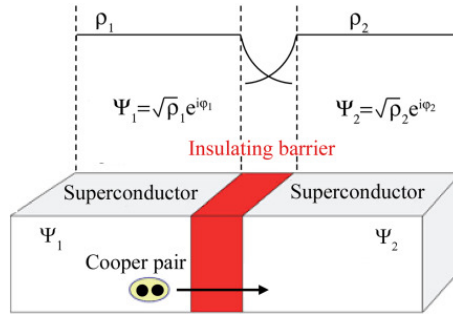


Figure 8: A simple schematic of a Josephson junction. The two superconducting electrodes are described by the macroscopic wavefunctions Ψ_1 and Ψ_2 .

First Josephson equation The first Josephson equation describes the current I flowing in the Josephson junction:

$$I = I_c \sin(\phi) \quad (6)$$

where I_c is a parameter of the junction called *critical current* and $\phi = \phi_2 - \phi_1$ is the phase difference between the two superconductors.

From equation 6, it is evident that even in the absence of an applied voltage across the Josephson junction, a non-zero current can flow, up to the critical current value I_c . This phenomenon is called *dc Josephson effect* and it is a direct consequence of the finite phase difference between the macroscopic wave functions in the two superconductors.

Second Josephson equation The second Josephson equation described the evolution of the phase difference ϕ :

$$\frac{\partial \phi}{\partial t} = \frac{2eV}{\hbar} \quad (7)$$

where V is the voltage applied across the junction.

From equation 7, we observe that a non-zero voltage across the Josephson junction generates an oscillating current across the junction. This is easily shown by integrating equation 7: $\phi(t) = \frac{2eV}{\hbar}t + \phi_0$, and inserting the term $\phi(t)$ in equation 6:

$$I(t) = I_c \sin\left(\frac{2eV}{\hbar}t + \phi_0\right) \quad (8)$$

Equation 8 describes the so called *ac Josephson effect*, generating an ac current when a voltage is applied.

Josephson inductance

The Josephson equations not only describe the dc and ac Josephson effects previously reviewed, but they also determine that the behaviour of a Josephson junction can be modelled as a non-linear inductance.

Starting from equation 6, we can write the time derivative as:

$$\frac{\partial I}{\partial t} = I_c \cos \phi \frac{\partial \phi}{\partial t} = \frac{2\pi I_c}{\Phi_0} V \cos \phi \quad (9)$$

where $\Phi_0 = h/2e$ is the flux quantum.

We observe that the time derivative of the current is proportional to a voltage, representing an inductive behaviour, according to the general definition of inductance L : $V = L \frac{\partial I}{\partial t}$. We can therefore define the *Josephson inductance* L_J and derive it from equation 9:

$$L_J(\phi) = \frac{\Phi_0}{2\pi I_c \cos \phi} = \frac{L_0}{\cos \phi} \quad (10)$$

where $L_0 = \frac{\Phi_0}{2\pi I_c}$.

Equation 10 shows that the Josephson inductance L_J non-linearly depends on the phase difference ϕ . The crucial consequence is that Josephson junctions can be used as a non-linear and tunable inductances in superconducting circuits. For this reason, Josephson junctions are probably the most important building blocks for quantum circuits such as tunable resonators, parametric amplifiers and qubits.

5 Microwave Tunable Resonators

In section 3, we have introduced two resonator configurations, namely the quarter-wave and the half-wave resonators. In both cases, the resonance frequency f_r depends only on the length l of the resonators, given the parameters L' and C' , and the boundary conditions of the resonators. For example, the resonance frequency of the fundamental mode of a quarter-wave resonator is:

$$f_0 = \frac{v_{\text{ph}}}{\lambda} = \frac{1}{4l\sqrt{L'C'}} \quad (11)$$

where $v_{\text{ph}} = 1/\sqrt{L'C'}$ is the phase velocity of the electromagnetic wave travelling in the resonator and λ is its wavelength.

Can we build a tunable resonator, i.e. a resonator whose resonance frequency is not fixed by the circuit geometry and can be tuned by means of an external parameters?

Looking at equation 11, we observe that to tune the resonance frequency we need to vary in a controlled way wither the length or the total inductance of the resonator or the total capacitance of the resonator.

In section 4, we have shown how a Josephson junction behaves as a tunable inductance, which therefore can be exploited to realise a tunable resonator. In the most common implementation of Josephson-junction based tunable resonators, a special circuit configuration including two Josephson junctions is used, called *dc SQUID* (*Superconducting Quantum Interference Device*).

A dc SQUID consist of a superconducting loop interrupted by two Josephson junctions, as shown in figure 9. The working principle of a SQUID is based on the dc Josephson effect introduced in section 4.

The detailed discussion of the physics of SQUID devices is beyond the scope of these lectures. A complete treatment can be found in the *The SQUID Handbook* (see section **Suggested Textbooks and Reviews**). For our purposes, we can treat a SQUID as a circuit component with an inductance L_{SQ} which periodically varies with the total magnetic flux Φ_{tot} threading the SQUID loop:

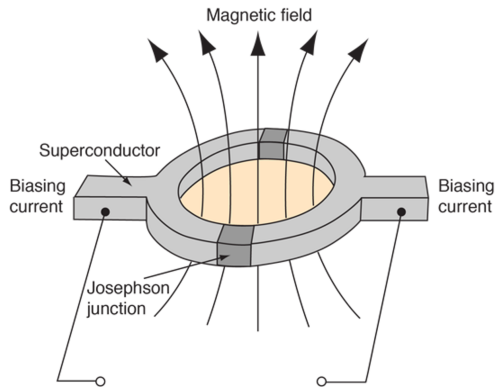


Figure 9: A schematic of a SQUID device, consisting of a superconducting loop with two Josephson junction in parallel. The SQUID response is periodically proportional to the magnetic flux threading the loop.

$$L_{\text{SQ}}(\Phi) = \frac{L_J}{2 \cos(\pi \Phi_{\text{tot}} / \Phi_0)} \quad (12)$$

where L_J is the inductance of the single Josephson junction, Φ_{tot} is the total flux through the SQUID loop and Φ_0 is the flux quantum. Note two important details related to equation 12:

- 1) We neglect the geometric inductance of the SQUID loop.
- 2) The total flux Φ_{tot} includes the externally applied magnetic flux Φ_{ext} as well as the flux induced by other currents biasing the SQUID, Φ_{b} , and smaller contributions from screening currents in the loop, Φ_{scr} . We can write the implicit relation: $\Phi_{\text{tot}} = \Phi_{\text{ext}} + \Phi_{\text{b}}(I) + \Phi_{\text{scr}}(\Phi_{\text{tot}})$. In the following we assume negligible bias currents and screening currents, so that $\Phi_{\text{tot}} \approx \Phi_{\text{ext}}$.

We can now integrate a SQUID in a quarter-wave resonator geometry, as shown in figure 10. The total inductance of the resonator circuit will then depend also on the SQUID inductance L_{SQ} and therefore a change in the external magnetic flux Φ_{ext} will affect the resonance frequency f_r :

$$f_r(\Phi_{\text{ext}}) = f_0 \left(1 + \frac{L_{\text{SQ}}(\Phi_{\text{ext}})}{L_r} \right) \quad (13)$$

where f_0 is the resonance frequency of the bare resonator, i.e. without the SQUID termination to ground, and L_r is the total inductance of the bare resonator, which is called *lumped-element inductance* and can be related to the distributed inductance L' . Note that also here we neglect the geometrical inductance of the SQUID loop.

In summary, using a dc SQUID as a tunable non-linear inductor integrated in a coplanar waveguide resonator, we have built a tunable resonator, whose resonance frequency can be externally controlled by tuning the magnetic flux threading the SQUID loop.

Figure 10 shows the circuit diagram and a microscope image of a tunable microwave resonator microfabricated in the FBK cleanroom facilities. A quarter-wave coplanar waveguide resonator is patterned from a 80 nm thick aluminium film and the two Josephson junctions forming the SQUID are visible. Next to the SQUID, a modulation line is present. By flowing current through the modulation line, we can induce a magnetic field in the SQUID loop, according to Biot–Savart law.

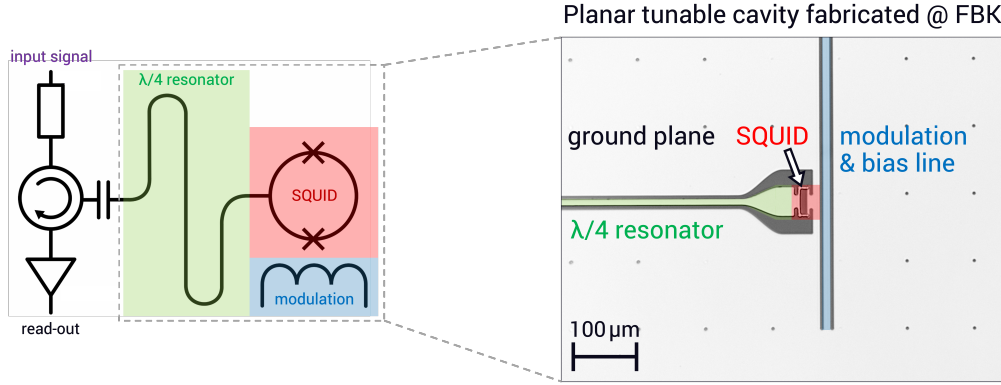


Figure 10: Circuit diagram and microscope image of a tunable resonator developed at FBK. The basic components of the spectroscopy apparatus used for the characterisation are also shown.

To characterise the tunable resonator, we cool the device down to ~ 10 mK temperature and we connected to an RF spectroscopy apparatus. At room temperature, we use a VNA to generate an input signal at port 1. The signal is routed from room temperature to the cryogenic stage, where the device is placed, and it is fed to the resonator through a circulator². The microwave signal reflected back by the tunable resonator, travels back through the circulator and is amplified on its way towards the room temperature stage. Finally, the output signal is connected to port 2 of the VNA. In this way, the response of the resonator is measured as a function of frequency, as previously shown in figure 7a.

This measurement is repeated while varying the dc current flowing through the modulation line, therefore effectively changing the magnetic flux through the SQUID loop. For each measurement, the resonance frequency $f_r = \omega_r/2\pi$ is extracted and can be plotted as a function of the magnetic flux, as shown in figure 11.

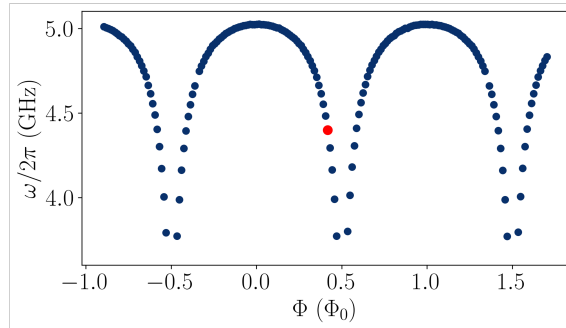


Figure 11: Experimental measurement of the modulation of the tunable resonator shown in figure 10. The resonance frequency is plotted as a function of the applied magnetic flux.

²A circulator is a microwave component with three ports, which allows transmission from port 1 to port 2, from port 2 to port 3 and from port 3 to port 1, in a circular fashion, while isolating the other directions. The circulator is shown in the schematic of figure 10.

6 Josephson Parametric Amplifiers

Amplifiers act as bridges between the quantum circuit sitting at cryogenic temperatures and the classic apparatus in the laboratory at room temperature that we intend to use for the read-out. In 1982, C. M. Caves was writing: “The last essential quantum mechanical stage of a measuring apparatus is a high-gain amplifier; it produces an output that we can lay our grubby, classical hands on.”.

When measuring a superconducting quantum circuit, we need to route the weak microwave output signal of the device from the cryogenic stage to the room temperature electronics and we need to amplify it. Typically, we use several amplification stages in cascade, as shown in the sketch of figure 12, and each amplifier inevitably adds noise.



Figure 12: Simple sketch of a cascade of amplifiers in series, each one characterised by a gain G_i .

The total system noise temperature T_{sys} of a chain of M amplifiers in series is given by the Friis formula:

$$T_{\text{sys}} = \sum_{i=1}^M \frac{T_{N,i}}{\prod_{j=1}^{i-1} G_j} = T_{N,1} + \frac{T_{N,2}}{G_1} + \frac{T_{N,3}}{G_1 G_2} + \dots \quad (14)$$

where the G_i is the gain of the i -th amplifier and $T_{N,i}$ is its noise temperature.

If the first amplifier has a large gain, i.e. $G_1 \gg 1$, the total system noise temperature is dominated by the noise performance of the first amplifier. Therefore, in order to maximise the signal-to-noise ratio, we need a first-stage-amplifier with a sufficiently high gain and as low noise as possible. Moreover, the insertion loss between the superconducting circuit and the amplifiers needs to be minimised. Thus, the amplifier is typically co-located with the superconducting circuit under test at the lowest temperature stage of the cryogenic apparatus, reducing as much as possible the number of contacts and components between the signal source and the amplifier.

Standard low-noise cryogenic amplifiers (e.g. HEMTs - High Electron Mobility Transistors) feature noise levels of a few Kelvin. Moreover, they dissipate too high power, if compared to the available cooling power in the cryogenic system. Ideally, we would like to use an amplifier with minimal power dissipation and with the lowest possible added noise, i.e. at the quantum noise limit.

Quantum noise limit

Any amplifier intrinsically adds noise. For any phase-preserving amplification process with gain G , the added noise can be expressed in terms of noise photons n_N :

$$n_N \geq \frac{|1 - 1/G|}{2}. \quad (15)$$

If the gain is small, $G \approx 1$, no noise is added. If the gain is large, $G \gg 1$, the number of added noise photons approaches $1/2$, the so called *standard quantum limit* (SQL). We often refer to this limit as *half-photon of noise*. The fundamental origin of such noise limit can be traced back to the manifestation of Heisenberg uncertainty principle. In this picture, the fluctuations in the two-quadrature-plane (I/Q-plane) must be limited to a minimal area corresponding to the zero-point fluctuations energy $\hbar f/2$.

We can translate a noise photon number n_N into a noise temperature T_N in units of Kelvin: $T_N = n_N \cdot hf/k_B$. For example, a quantum-limited amplifier operating at 5 GHz has a noise temperature $T_N = 1/2 \cdot h \cdot (5 \text{ GHz})/k_B = 0.12 \text{ K}$.

Superconducting parametric amplifier can feature minimal noise, reaching the standard quantum limit, and can operate with very small power dissipation, making them particularly interesting for cryogenic quantum-limited read-out of superconducting devices, such as qubits.

Parametric amplification

Any non-linear system where we can periodically modulate a parameter of the system (e.g. a circuit reactance), converting energy between conjugate field variables of the system (e.g. voltage and current), can produce a parametric behaviour. The simplest example of parametric amplification is a child on a swing, as shown in figure 13(left), where the potential is at the first order quadratic in displacement. The child is squatting at twice the frequency of the swing oscillations, therefore modulating the position of the centre of mass and achieving parametric gain in the oscillation amplitude. The parametric periodic modulation is often called *pumping* and the condition for parametric gain is $f_p \approx 2f_0$, where f_p is the pumping frequency and f_0 is the natural oscillator frequency.

Another curious example of parametric amplification is the famous Botafumeiro, a thurible used at the Santiago de Compostela Cathedral, in Spain. The Botafumeiro is suspended 20 m from a pulley mechanism under the dome on the roof of the church and it swings in a 65 m arc. The maximum amplitude of the oscillation is reached by parametric amplification, modulating the length of the suspension rope at twice the oscillation frequency. This modulation (*pumping*) effectively injects energy into the system, producing gain in the oscillation amplitude. Enjoy the video here: <https://www.youtube.com/watch?v=beP8N9X0nyw>.

We can implement parametric amplification in a non-linear LC resonator circuit, like the one sketched in figure 13(right), by pumping the inductance or the capacitance of the system. The tunable resonator discussed in section 5 is exactly the circuit we need for this, since its energy is at first order quadratic in the magnetic flux in the inductor and we can pump the SQUID inductance by modulating the magnetic flux through the SQUID.

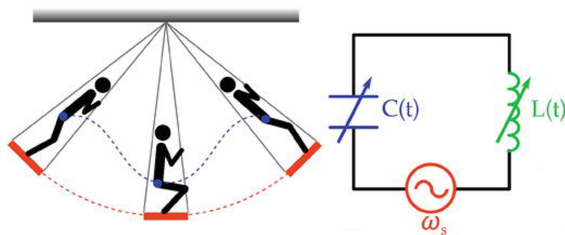


Figure 13: Two analogous examples of parametric amplification: the child on the swing, amplifying the oscillation amplitude by pumping the moment of inertia (left) and an LC resonator circuit, where the signal ω_s is amplified by pumping the magnetic flux in the inductor $L(t)$ or the electrical charge in the capacitor $C(t)$.

Flux-driven JPA

A flux-driven Josephson Parametric Amplifier (JPA) consists of a quarter-wave coplanar waveguide resonator terminated to ground by a dc SQUID, as shown in figure 10 and in figure 15(a). As previously discussed, the dc SQUID acts as a flux-tunable non-linear inductance $L_{SQ}(\Phi_{ext})$ which affects the resonance frequency of the circuit $f_r = 2\pi\omega_r$, as described by equation 13. We have already seen in section 5 how this circuit functions as a tunable microwave resonator. We can also operate the same circuit as a flux-driven JPA, inducing parametric amplification by periodically modulating (pumping) the inductance L_{SQ} . The parametric modulation (pump) must be at a

frequency $\omega_p \approx 2\omega_r$, i.e. close to twice the resonance frequency of the circuit.

By pumping we induce a *three-wave mixing* process, where an input signal tone is amplified if its frequency ω_s is close to the resonance frequency of the circuit, meaning close to half the pump frequency ω_p . This condition can be written as:

$$\omega_s = \omega_p/2 + \delta\omega \quad (16)$$

where $\delta\omega$ is the detuning from the resonance frequency. Because of energy conservation, another tone called *idler* is created at a frequency

$$\omega_i = \omega_p/2 - \delta\omega. \quad (17)$$

Therefore, the condition for a three-wave mixing process can be written as:

$$\omega_p = \omega_s + \omega_i. \quad (18)$$

We can visualise the three-wave mixing process as the conversion of one pump photon into one signal photon and one idler photon, as shown in figure 14a. In this picture, it is clear how the generation of the idler photon is required by energy conservation. Thanks to this conversion from pump photons to signal photons, we effectively achieve an amplification of the signal.

The detuning $\delta\omega$ should be sufficiently small, such that the signal frequency ω_s falls within the line-width of the resonance of the circuit, as shown in figure 14b. If the detuning is zero, $\delta\omega = 0$, i.e. if $\omega_s = \omega_r$, signal and idler will be at the same frequency, $\omega_s = \omega_i = \omega_p/2$. This case is called *degenerate parametric amplification*.

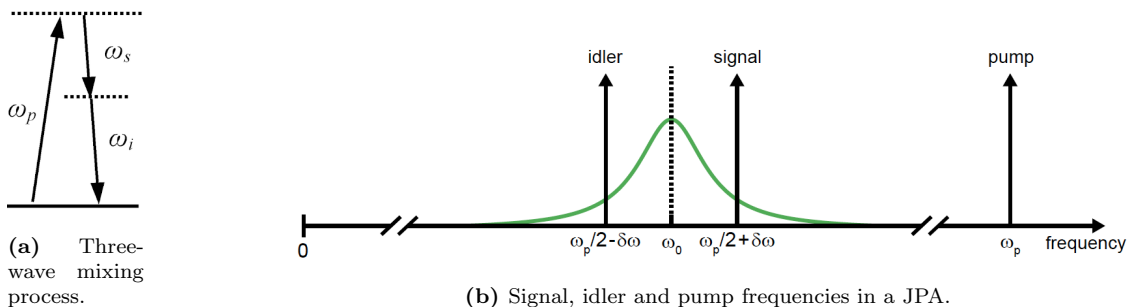


Figure 14: Three-wave mixing process in a flux-driven JPA and distribution of the relevant frequencies, namely signal, idler and pump. The pump frequency is at twice the resonance frequency of the JPA ω_0 . The green curve shows the shape of the resonance of the circuit.

JPA operation The operation of a flux-driven JPA is schematically represented in figure 15. After having chosen a flux working point, as shown in figure 15(b), a strong pump signal at frequency $2f_0$, where f_0 is the resonance frequency of the circuit, is injected into the pump port, modulating the flux through the dc SQUID. An input signal with amplitude A at frequency $f_0 - f$ is injected in the resonator circuit and read out in reflection. As a result of the parametric process, the input signal is amplified with a gain G and an idler mode appears at frequency $f_0 + f$.

Degenerate amplification and squeezing In the special case of degenerate amplification, signal and idler are at the same frequency and therefore they can interfere constructively or destructively, depending on their phases. Thus, the gain of the amplification process becomes sensitive to the relative phase between signal and idler modes. By tuning the phase, deamplification or amplification can be achieved. In the case of deamplification, the quadrature fluctuations can be squeezed below those of the vacuum. It is therefore possible to overcome the standard quantum limit, but only on one quadrature of the signal.

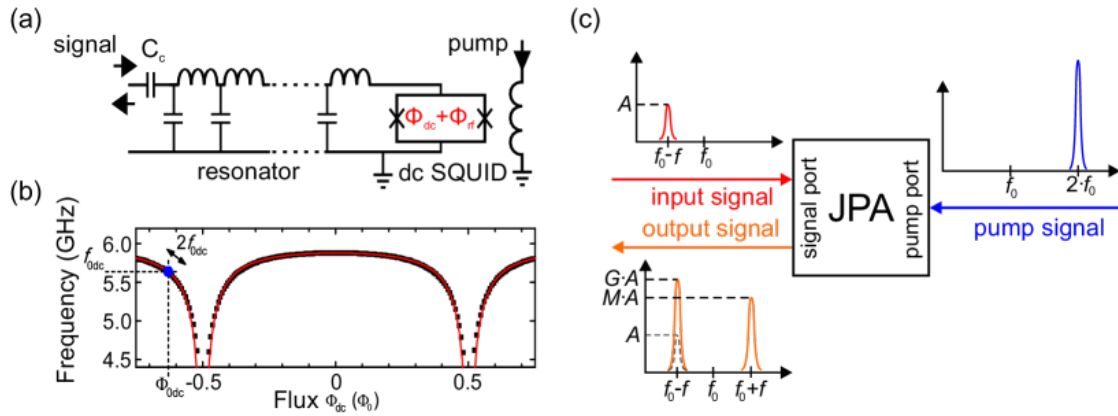


Figure 15: (a) Circuit diagram of a flux-driven JPA. (b) Dependence of the resonant frequency on the flux. The operation point is marked in blue. (c) Schematic of the operating principle of the JPA. Figure from L. Zhong et al., *Squeezing with a flux-driven Josephson parametric amplifier* New J. Phys. 15 125013, 2013.

In conclusion, a flux-driven JPA exploits three-wave mixing to achieve parametric amplification by pumping the SQUID inductance. JPAs have demonstrated amplification at the quantum noise limit with high gain, $G \geq 20$ dB, and for this reason they are often used as first amplifiers in cryogenic set-ups for the read-out of superconducting quantum circuits. The main limitation of JPAs is their small amplification bandwidth, which is typically limited to a few MHz.

To obtain larger amplification bandwidth, which is crucial for example to read-out arrays of qubits or arrays of cryogenic detectors, another category of superconducting parametric amplifiers is currently developed, namely the Travelling Wave Parametric Amplifiers (TWPAs). The fundamental difference between a JPA and a TWPAs is that the former is a resonant circuit while the latter is a transmission line. TWPAs have demonstrated near quantum-limited amplification with bandwidths up to several GHz. The discussion of TWPAs is however beyond the scope of these lectures. Both JPAs and TWPAs can be used as amplifiers as well as squeezers, for the generation of entangled microwave photons. The physics of squeezed states and entanglement generation is of high interest for quantum optics experiments in the microwave regime.

7 Superconducting Qubits

The non-linearity offered by Josephson junctions integrated in microwave circuits is not only useful to build parametric amplifiers, as described in section 6, but also to realise superconducting qubits. A qubit is by definition a two-level system displaying a quantum mechanical behaviour. The two energy levels are used as a basis for computation, exploiting the fact that the qubit can be in a coherent superposition of multiple states.

As any other quantum mechanical system, the time evolution of a qubit is governed by the Schrödinger equation:

$$\hat{H} |\psi(t)\rangle = i\hbar \frac{\partial}{\partial t} |\psi(t)\rangle \quad (19)$$

where $|\psi(t)\rangle$ is the state of the quantum system at time t and \hat{H} is the Hamiltonian quantum operator. Determining the Hamiltonian of the system is required to derive its dynamics.

Quantum harmonic oscillator

To understand the physics of superconducting qubits, it is natural to start from the classical description of the simplest quantum circuit we can think of, namely a linear harmonic oscillator. We can implement such system with an LC resonator, as shown in figure 16a, where the energy of the system is oscillating between the magnetic energy in the inductor L and the electrical energy in the capacitor C .

The classical Hamiltonian of the LC resonator is given by:

$$H = \frac{Q^2}{2C} + \frac{\Phi^2}{2L} = \frac{1}{2}CV^2 + \frac{1}{2}LI^2 \quad (20)$$

where Q and Φ are the generalised circuit coordinates, charge and flux, respectively.

By definition, the flux Φ is the integral of the voltage V : $\Phi(t) = \int V(t')dt'$ and the charge Q is the integral of the current I : $Q(t) = \int I(t')dt'$. We also should remember that $V = LdI/dt$ and $I = CdV/dt$.

We can interpret the electrical energy as the kinetic energy and the magnetic energy as the potential energy of the oscillator, in analogy with a mechanical oscillator. In this analogy, the usual conjugate variables to describe a mechanical oscillators, position x and momentum p , are mapped to charge Q and flux Φ . The Hamiltonian in equation 24 is analogous to that of mechanical harmonic oscillator, with mass $m = C$ and momentum p . Expressed in position x and momentum p , the Hamiltonian reads $H = p^2/2m + m\omega^2x^2/2$.

To migrate from a classical to a quantum description, we introduce the quantum operators $\hat{\Phi}$ and \hat{Q} which satisfy the commutation relation $[\hat{\Phi}, \hat{Q}] = i\hbar$. The operators hats are omitted in the following for simplicity.

We define the reduced flux $\phi := 2\pi\Phi/\Phi_0$ and the reduced charge $n := Q/2e$, which obey the commutation relation $[\phi, n] = i$. The quantum-mechanical Hamiltonian can then be derived:

$$H = 4E_C n^2 + \frac{1}{2}E_L \phi^2 \quad (21)$$

where $E_C = e^2/(2C)$ is the charging energy necessary to add a Cooper pair to the capacitor island and $E_L = (\phi_0/2\pi)^2/L$ is the inductive energy. The quantum operator n corresponds to the excess number of Cooper pairs on the island in the circuit shown in figure 16a. The reduced flux ϕ corresponds to the phase across the inductor.

In a more compact form, we can write the Hamiltonian of the quantum harmonic oscillator as:

$$H = \hbar\omega \left(a^\dagger a + \frac{1}{2} \right) \quad (22)$$

where a^\dagger and a are the creation and annihilation operators of a single excitation of the resonator.

Non-linearity and anharmonicity The quantum harmonic oscillator features quantised and equidistant energy levels, as shown in figure 16b. However, such system cannot be used as a qubit. The main limitation is in fact the difficulty in defining and addressing a computation subspace consisting of only two energy states. Typically the ground state $|0\rangle$ and the first excited state $|1\rangle$ are exploited. The transition between these two energy levels should be driven without exciting other levels. Due to the quadratic potential of the quantum harmonic oscillator with equidistant energy levels, the two levels belonging to the computation subspace cannot be addressed independently from the others. To lift this degeneracy, a non-linear element needs to be integrated in the circuit.

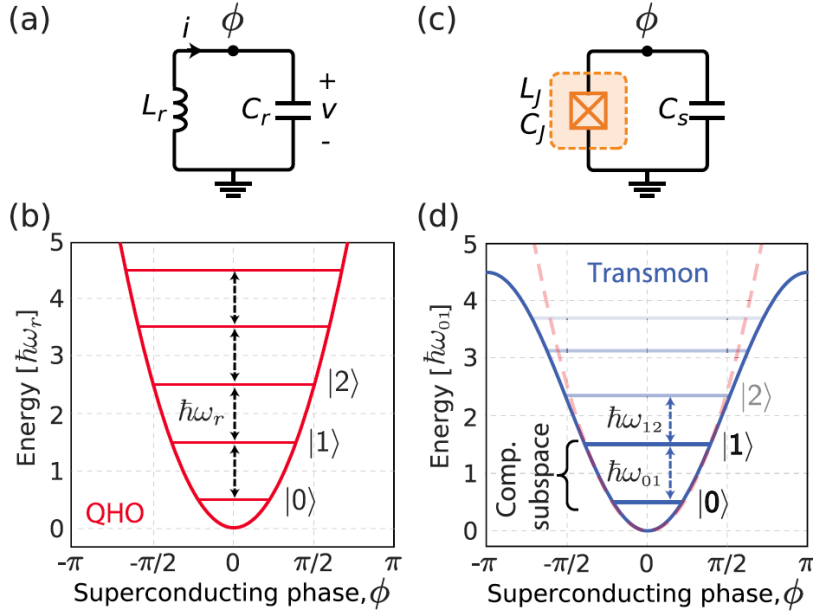


Figure 16: (a) Circuit for a parallel LC oscillator (quantum harmonic oscillator, QHO). (b) Energy potential for the QHO, where energy levels are equidistantly spaced. (c) Qubit circuit with a non-linear inductance given by the Josephson junction. (d) Quadratic energy potential (dashed red) reshaped to a sinusoidal potential (solid blue) by the non-linearity of the Josephson junctions, yielding to non-equidistant energy levels. Figure from P. Krantz et al., *A quantum engineer's guide to superconducting qubits*, Appl. Phys. Rev. 6(2): 021318, 2019.

The charge qubit and the transmon qubit

By introducing a Josephson junction, which acts as a non-linear inductance, as discussed in section 4, we are able to deform the potential and make the oscillator anharmonic, as shown in figure 16d. The parabolic (i.e. quadratic) potential of the harmonic oscillator becomes cosinusoidal. This results in non-equidistant energy levels, allowing for the needed selectivity of individual transitions between the levels, without involving higher non-computational states.

A high anharmonicity, i.e. a high difference in the transition frequencies between levels, $0 \rightarrow 1$, $1 \rightarrow 2$, ..., is preferable to build superconducting qubits. Practically, the amount of anharmonicity sets a limit on how short the pulses used to control the qubit can be.

We replace the linear inductor in the harmonic oscillator (figure 16a) with a Josephson junction, i.e. a non-linear inductance (figure 16b). The resulting anharmonic oscillator can be used as a qubit and its Hamiltonian becomes:

$$H = 4E_C n^2 - E_J \cos \phi \quad (23)$$

where $E_C = e^2/(C_s + C_J)$ with C_s the shunt capacitor and C_J the self-capacitance of the Josephson junction, and $E_J = I_c \Phi_0/2\pi$.

We can explicit a term $n_g = Q_g/2e$ representing a possible offset charge due to an external electric field bias, such that equation 23 becomes:

$$H = 4E_C(n - n_g)^2 - E_J \cos \phi. \quad (24)$$

Such external electric field can arise from spurious unwanted processes in the qubit environment or from an intentional external gate voltage.

The dynamics of the system is governed by the dominant energy in the Hamiltonian of equation 24. In particular, the relevant parameter is given by E_J/E_C , which is the ratio between the Josephson energy E_J and the charge energy E_C .

The charge qubit If the charging energy E_C dominates, i.e. $E_J/E_C \leq 1$, the eigenstates of the Hamiltonian are approximately matching the eigenstates of the charge operator n . This configuration is often referred as *charge qubit*. In this situation, the qubit becomes highly sensitive to charge noise. In other words, a small change in gate charge n_g has a large impact on the transition frequencies of the energy levels, as shown in figure 17. We can refer to this condition as large *charge dispersion*. As a result, unavoidable charge fluctuations in the environment lead to fluctuations in the qubit transition frequency and to dephasing.

The transmon qubit To lower the charge dispersion, we can increase the ratio E_J/E_C to values in the order of 50-80, as shown in figure 17. In this way, the Josephson energy dominates and the the charge degree of freedom becomes highly delocalised. The regime with $E_J/E_C \gg 1$ is called *transmon regime*. In this regime, the charge dispersion decreases exponentially with E_J/E_C . The price to pay is a reduced anharmonicity $\alpha = E_{12} - E_{01}$. However, the anharmonicity is weakly decreasing with E_J/E_C , following the dependance $\alpha \sim (E_J/E_C)^{-1/2}$. Therefore, the charge dispersion is reduced much faster than the anharmonicity by increasing E_J/E_C .

The transmon qubit is one of the most popular superconducting qubit configurations, since the reduced charge dispersion allows for longer coherence times, even if with a reduced anharmonicity. To access the transmon regime, we can decrease E_C in order to increase the ratio E_J/E_C . To achieve this, in the typical transmon designs, the Josephson junction is shunted with a large capacitor, $C_s \gg C_J$.

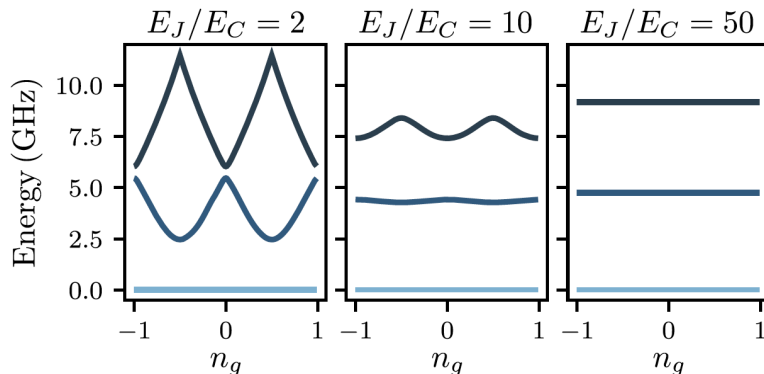


Figure 17: Frequency difference of the first three energy levels of the a charge qubit in different regimes as a function of the offset charge. Figure from A. Blais et al., *Circuit quantum electrodynamics*, Rev. Mod. Phys. 93, 025005, 2021.

Flux-tunable transmon In order to add tunability to the transmon circuit shown in figure 16(c), the single Josephson junction can be replaced by a SQUID, i.e. by two Josephson junctions in parallel. In this way, the transmon frequency can be tuned by changing the flux Φ_{ext} threading the SQUID loop. Here, Φ_{ext} is the external flux applied to the SQUID, which corresponds to the total flux threading the SQUID loop in the approximation of negligible flux induced by other effects. The transmon Hamiltonian for a flux-tunable transmon is:

$$H = 4E_C n^2 - E_{J1} \cos \phi_1 - E_{J2} \cos \phi_2 \quad (25)$$

where E_{Ji} is the Josephson energy of the i -th junction and ϕ_i is the phase difference across the i -th junction. We neglect the geometric inductance of the SQUID loop.

Because of flux quantisation, we have that $\phi_1 - \phi_2 = 2\pi\Phi_{\text{ext}}/\Phi_0 \pmod{2\pi}$. We can define the average phase difference $\phi = (\phi_1 + \phi_2)/2$ and rewrite the Hamiltonian as:

$$H = 4E_C n^2 - E_J(\Phi_{\text{ext}}) \cos(\phi - \phi_0) \quad (26)$$

where

$$E_J(\Phi_{\text{ext}}) = (E_{J1} + E_{J2}) \cos\left(\frac{\pi\Phi_{\text{ext}}}{\Phi_0}\right) \sqrt{1 + \phi_0^2}. \quad (27)$$

Here, $\phi_0 = d \tan(\pi\Phi_{\text{ext}}/\Phi_0)$ represents an effective phase due to the external flux and $d = (E_{J1} - E_{J2})/(E_{J1} + E_{J2})$ is the asymmetry between the two Josephson junctions forming the SQUID. For a time-independent flux, the phase ϕ_0 can be neglected and equation 28 reduces to:

$$E_J(\Phi_{\text{ext}}) = (E_{J1} + E_{J2}) \cos\left(\frac{\pi\Phi_{\text{ext}}}{\Phi_0}\right). \quad (28)$$

Therefore, in a flux-tunable transmon, we have a Josephson energy $E_J(\Phi_{\text{ext}})$ which can be tuned with the external applied magnetic flux. This results in a flux-tunable transmon frequency ω_q given by:

$$\omega_q(\Phi_{\text{ext}}) = \sqrt{8E_C |E_J(\Phi_{\text{ext}})|} - E_C/\hbar^3. \quad (29)$$

The possibility of tuning the transmon frequency by large values, up to 1 GHz, in a fast way, down to 10 ns, is relevant for example for the implementation of quantum logic gates. However, this additional degree of freedom can lead to dephasing due to flux noise. Flux-tunable transmons with asymmetric Josephson junctions, $d \neq 0$, feature less tunability and, therefore, suffer less from flux noise.

Resonator coupling

Transmons are rather large objects, because of their large capacitance and, therefore, they can naturally be capacitively coupled to microwave resonators. A schematic representation is shown in figure 18. The electric field of the resonator acts as a gate voltage, taking the place of the offset charge operator n_g : $n_g \rightarrow -n_r$. Note that the choice of sign is arbitrarily.

We can write the Hamiltonian of the combined system, comprising the transmon and the resonator, as:

$$H = 4E_C(n + n_r)^2 - E_J \cos \phi + \sum_m \hbar\omega_m a_m^\dagger a_m \quad (30)$$

where $n_r = \sum_m n_m$ with $n_m = (C_g/C_m)/2e$ is the contribution of the offset charge term due to the m th resonator mode. C_g is the gate capacitance and C_m is the capacitance of the associated resonator mode. We assume a small gate capacitance C_g .

We can apply the so called *single-mode approximation*, assuming that the transmon frequency is much closer to one of the resonator modes than all the other modes. Therefore, we can truncate the sum in equation 30 to a single term. Under this condition, the Hamiltonian reduces to a single

oscillator of frequency ω_r coupled to a transmon qubit of frequency ω_q . The oscillator can always be represented by a lumped-element LC circuit, even if it consists of a 3D cavity, as shown in figure 18.

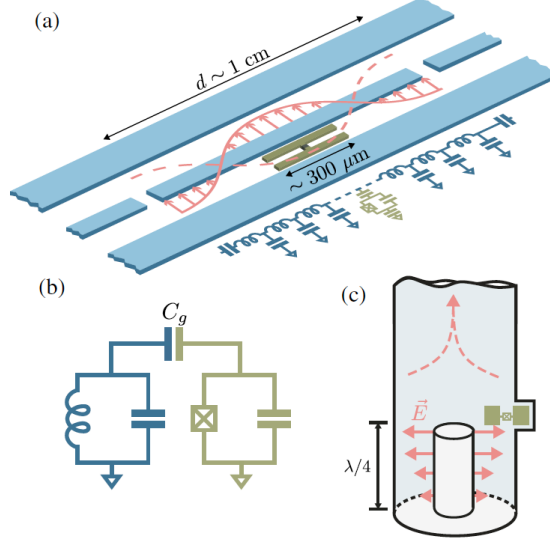


Figure 18: Schematic representation of a qubit (green) coupled to a resonator. The resonator can be a planar resonator (a), a general lumped-element LC circuit (b) and a 3D cavity (c). Figure from A. Blais et al., *Circuit quantum electrodynamics*, Rev. Mod. Phys. 93, 025005, 2021.

The Hamiltonian in the single-mode approximation becomes:

$$H \approx \hbar\omega_r a^\dagger a + \hbar\omega_q b^\dagger b - \frac{E_C}{2} b^\dagger b^\dagger b b - \hbar g (b^\dagger - b)(a^\dagger - a) \quad (31)$$

where ω_r is the frequency of the mode of interest and g is the oscillator-transmon coupling constant, also called *light-matter* coupling constant.

In the experimentally relevant situation where $|g| \ll \omega_r, \omega_q$, meaning that the coupling constant is much smaller than the frequencies of the systems, the Hamiltonian in equation 31 simplifies to

$$H \approx \hbar\omega_r a^\dagger a + \hbar\omega_q b^\dagger b - \frac{E_C}{2} b^\dagger b^\dagger b b + \hbar g (b^\dagger a + b a^\dagger). \quad (32)$$

If we restrict the description to the first two levels of the transmon, i.e. the ground state $|g\rangle$ and the first excited state $|e\rangle$, we can define:

$$\sigma_+ = |e\rangle \langle g|; \quad \sigma_- = |g\rangle \langle e|; \quad \sigma_z = |e\rangle \langle e| - |g\rangle \langle g| \quad (33)$$

and we can replace in equation 31 $b^\dagger \rightarrow \sigma_+$ and $b \rightarrow \sigma_-$.

In this way, we obtain the well-known *Jaynes-Cummings Hamiltonian*:

$$H_{JC} = \hbar\omega_r a^\dagger a + \frac{\hbar\omega_q}{2} \sigma_z + \hbar g (a^\dagger \sigma_- + a \sigma_+). \quad (34)$$

The Jaynes-Cummings Hamiltonian is widely used in circuit QED and cavity QED. It models the interaction of a two-level atom with a quantised mode of an optical cavity. In our case, the transmon is an artificial atom and it interacts with the mode of the microwave resonator. In particular, the last term of equation 34 describes the coherent exchange of a single quantum between light and matter, here realized as a microwave photon in the resonator or an excitation of the artificial atom.

Suggested Textbooks and Reviews

Richard Feynman, *The Schrödinger Equation in a Classical Context: A Seminar on Superconductivity*, Caltech https://www.feynmanlectures.caltech.edu/III_21.html

Antonio Barone, Gianfranco Paternò, *Physics and Applications of the Josephson Effect*, ISBN:9780471014690, 1982

John Clarke and Alex I. Braginski, *The SQUID Handbook: Fundamentals and Technology of SQUIDs and SQUID Systems*, 2004

A. M. Zagoskin, *Quantum Engineering - Theory and Design of Quantum Coherent Structures*, Cambridge University Press, 2011

A. Blais, A. L. Grimsmo, S. M. Girvin and A. Wallraff, *Circuit quantum electrodynamics*, Rev. Mod. Phys. **93**, 025005, 2021